Earth's Future

Responses of global terrestrial evapotranspiration to climate change and increasing atmospheric CO_2 in the 21st century

Shufen Pan[1], Hanqin Tian[1], Shree R.S. Dangal[1], Qichun Yang[1], Jia Yang[1], Chaoqun Lu[1], Bo Tao[1], Wei Ren[1], and Zhiyun Ouyang[2]

[1]International Center for Climate and Global Change Research, School of Forestry and Wildlife Sciences, Auburn University, Auburn, Alabama, USA, [2]State Key Laboratory of Urban and Regional Ecology, Research Center for Eco-Environmental Sciences, Chinese Academy of Sciences, Beijing, China

Abstract Quantifying the spatial and temporal patterns of the water lost to the atmosphere through land surface evapotranspiration (ET) is essential for understanding the global hydrological cycle, but remains much uncertain. In this study, we use the Dynamic Land Ecosystem Model to estimate the global terrestrial ET during 2000–2009 and project its changes in response to climate change and increasing atmospheric CO_2 under two IPCC SRES scenarios (A2 and B1) during 2010–2099. Modeled results show a mean annual global terrestrial ET of about 549 (545–552) mm yr^{-1} during 2000–2009. Relative to the 2000s, global terrestrial ET for the 2090s would increase by 30.7 mm yr^{-1} (5.6%) and 13.2 mm yr^{-1} (2.4%) under the A2 and B1 scenarios, respectively. About 60% of global land area would experience increasing ET at rates of over 9.5 mm $decade^{-1}$ over the study period under the A2 scenario. The Arctic region would have the largest ET increase (16% compared with the 2000s level) due to larger increase in temperature than other regions. Decreased ET would mainly take place in regions like central and western Asia, northern Africa, Australia, eastern South America, and Greenland due to declines in soil moisture and changing rainfall patterns. Our results indicate that warming temperature and increasing precipitation would result in large increase in ET by the end of the 21st century, while increasing atmospheric CO_2 would be responsible for decrease in ET, given the reduction of stomatal conductance under elevated CO_2.

1. Introduction

The global water cycle of the 20th century has intensified, and the rate of intensification for the 21st century is expected to accelerate due to climate change [*Durack et al.*, 2012]. This intensification shows that wet areas are getting wetter and dry areas are getting drier [*Trenberth*, 2011]. To better understand the hydrological intensification in the future, we need to accurately estimate major components of the global hydrological budget. Evapotranspiration (ET) is considered to be one of the most significant processes of the hydrological cycle as it returns about 60% of global land surface precipitation and consumes more than half of absorbed solar radiation [*Trenberth et al.*, 2009]. Although great efforts have been devoted to investigate terrestrial ET variability across multi-spatial scales in the contemporary period [*Cleugh et al.*, 2007; *Jung et al.*, 2010; *Zeng et al.*, 2012], how terrestrial ET would be further altered by future climate conditions has not yet been well investigated.

The Intergovernmental Panel on Climate Change (IPCC) assessment indicated that global average temperature has increased by 0.74°C since the pre-industrial times and that this trend is expected to continue during the rest of the 21st century [*IPCC*, 2007]. Additionally, atmospheric CO_2 concentration has increased from the pre-industrial level of 280 to 379 ppm in 2005 [*IPCC*, 2007]. Global mean temperature is projected to increase by 4.6°C by the 2090s compared with that of the 2000s under the high emission scenario (A2), while global annual precipitation would increase by 16.9%. Projected changes in atmospheric CO_2 concentration showed large increases under the A2 scenario, from 379.6 ppm in the 2000s to 809 ppm in the 2090s, which is equivalent to an overall increase of 114.9%. Such dramatic changes in climate and atmospheric composition would profoundly affect terrestrial ET. Therefore, a quantitative investigation of terrestrial ET responses to future climate and atmospheric CO_2 scenarios is necessary and important to our understanding of future terrestrial water cycling and water resource management [*Arnell*, 1999; *Farley et al.*, 2005].

Observational and experimental evidences have shown that both climate and atmospheric CO_2 concentration affect terrestrial ET. Climate factors that influence ET include solar radiation, precipitation, wind speed, and temperature. Climate factors control both water vapor demand and moisture supply for ET. Air temperature affects the potential ET (PET) by regulating the air moisture holding capacity and determining the potential water fluxes from the soil to the atmosphere [*Allen et al.*, 1998]. Precipitation affects ET by controlling soil water content [*Jung et al.*, 2010]. In some land ecosystems where precipitation is the primary source of soil moisture, actual ET (AET) is significantly controlled by precipitation [*Kurc and Small*, 2004]. Interactions of these two climate factors affect the spatial variations of ET over large areas. In addition to temperature and precipitation, elevated atmospheric CO_2 is another factor that may induce changes in ET [*Allen*, 1991]. A growing body of evidence in literature suggests that elevated atmospheric CO_2 concentration acts to stimulate plant growth, thereby increasing the area of transpiring leaves, which enhances ET [*Cao et al.*, 2010; *Felzer et al.*, 2009; *Piao et al.*, 2010]. But this view has been questioned by other studies showing that plants subjected to elevated CO_2 concentration close their stomata partially and reduce transpiration. Results from elevated CO_2 treatment experiments showed that elevated CO_2 concentration tends to increase stomatal resistance and leads to a partial closure of the stomatal apertures [*Baker et al.*, 1990; *Shams et al.*, 2012].

Measurements and observations of ET in the field have been widely conducted across different terrestrial ecosystems [*Price*, 2011], but it is difficult to directly measure ET over a large region. Developments of satellite and geographic information technologies have provided spatially and temporally explicit estimates of land surface ET at regional and global scales [*Jung et al.*, 2010; *Mu et al.*, 2007]. However, neither field observations nor satellite-based approaches can quantify the relative roles of climate and CO_2 in controlling terrestrial ET.

Numerical modeling has played an important role in simulating terrestrial ET since the 1970s [*Alton et al.*, 2009; *Liu et al.*, 2013; *Mu et al.*, 2011]. Model simulation experiments provide a possible solution for quantifying the contributions of different environmental factors on ET [*Liu et al.*, 2013; *Shi et al.*, 2013]. In our previous studies, we have used a fully distributed land ecosystem model – the Dynamic Land Ecosystem Model (DLEM) [*Tian et al.*, 2010b] to evaluate the spatial and temporal patterns of terrestrial ET and runoff in response to multiple environmental factors including climate, CO_2, land use, and nitrogen deposition across different regions of the world [*Liu et al.*, 2008; *Liu et al.*, 2013; *Yang et al.*, 2014]. In this study, we used the DLEM 2.0 to estimate the contemporary global terrestrial ET patterns in the first decade of the 21st century and project future ET change for the rest of this century in response to climate change and increasing atmospheric CO_2. The purpose of this study is to: (1) provide the contemporary estimate of global terrestrial ET during 2000–2009; (2) project global terrestrial ET response to climate change and increasing CO_2 concentration during 2010–2099 under IPCC SRES emission scenarios (A2 and B1); (3) investigate the spatial and temporal patterns of global ET as well as the responses of different biomes to climate change and increasing CO_2; and (4) assess the uncertainties of future global ET under different emission scenarios.

2. Methods

2.1. The Dynamic Land Ecosystem Model

The DLEM is a process-based ecosystem model driven by environmental changes in climate, atmospheric compositions including CO_2, nitrogen deposition and ozone (O_3), land use and land cover (LULC), and land management practices to simulate the structural and functional dynamics of terrestrial ecosystems. The DLEM has five core components: (1) biophysics, (2) plant physiology, (3) soil biogeochemistry, (4) dynamic vegetation, and (5) land use and management [*Tian et al.*, 2010b]. The DLEM has been extensively calibrated at stand and regional scales for different biomes (forest, grassland, and cropland) by using the data from the Chinese Ecological Research Network, US Long-term Ecological Research (LTER) sites, and AmeriFlux network [*Pan et al.*, 2014a; *Pan et al.*, 2014b; *Ren et al.*, 2012; *Tian et al.*, 2011a; *Tian et al.*, 2011b]. Recently, the DLEM has been updated to DLEM 2.0 to account for multiple soil layer processes, and the dynamic linkage between terrestrial and riverine ecosystems. The detailed description of how the DLEM simulates terrestrial ET is available in *Liu et al.* [2013] and *Yang et al.* [2014]. Below we provide a brief description of these processes.
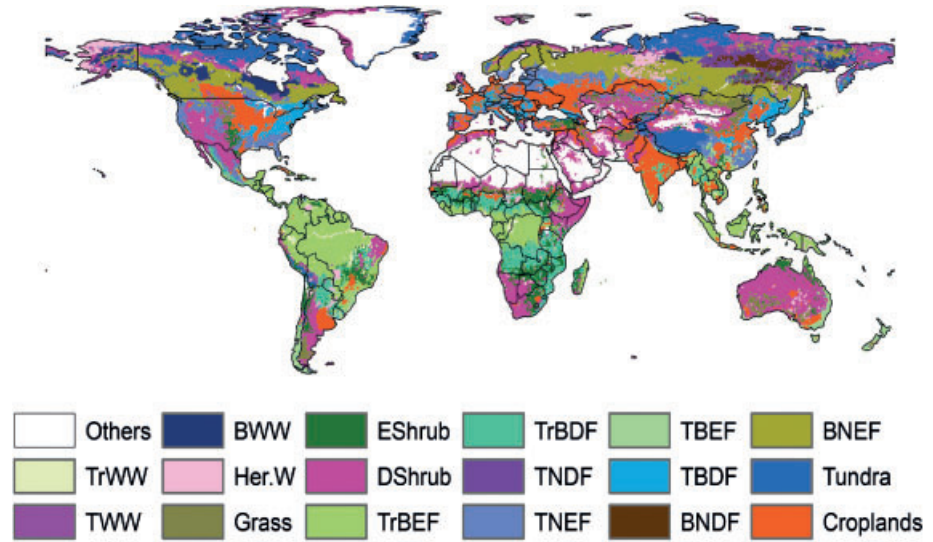
Figure 1. Contemporary vegetation map of the world as observed from DLEM for the year 2010. TrWW: tropical woody wetlands; TWW: temperate woody wetlands; BWW: boreal woody wetlands; Her. W: herbaceous wetlands; EShurb: evergreen shrubs; DShrub: deciduous shrubs; TrBEF: tropical broadleaf evergreen forest; TrBDF: tropical broadleaf deciduous forest; TNDF: temperate needleleaf deciduous forest; TNEF: temperate needleleaf evergreen forest; TBEF: temperate broadleaf evergreen forest; TBDF: temperate broadleaf deciduous forest; BNDF: boreal needleleaf deciduous forest; BNEF: boreal needleleaf evergreen forest; Others: desert and ice.

Plant transpiration in DLEM 2.0 is calculated with the Penman–Monteith equation [*Wigmosta et al.*, 1994]. In the model canopy conductance and resistance are up-scaled from the two-big-leaf model.

$$E_t = \frac{\Delta R_n + \rho c_P \left(e_s - e\right) \left(g_c\right)_j}{\lambda_v \left(\Delta + \gamma \left(1 + \left(g_c\right)_j / \left(g_s\right)_j\right)\right)} \tag{1a}$$

$$\left(g_c\right)_j = \frac{LAI_j^{sun}}{\left(r_s^{sun}\right)_j} + \frac{LAI_j^{sha}}{\left(r_s^{sha}\right)_j} \tag{1b}$$

$$LAI_j^{sun} = 2 \cos \theta_{ave} \left(1 - e^{-0.5 \Omega LAI / \cos \theta_{ave}}\right) \tag{2a}$$

$$LAI^{sha} = LAI - LAI_j^{sun} \tag{2b}$$

Where E_t is the water transpiration rate (m^3 s^{-1} m^{-2}); Δ is the slope of the saturated vapor pressure–temperature curve (Pa k^{-1}); R_n is the net radiation flux density (W m^{-2}); ρ is the air density (kg m^{-3}); λv is the latent heat for water vaporization (J g^{-1}); γ is the psychrometric constant; j is the jth plant functional type (PFT; Figure 1); g_c and g_s are the canopy conductance and stomatal conductance, respectively (m s^{-1}); r_s^{sun} and r_s^{sha} are the stomatal resistance of sunlit leaves and shaded leaves (s m^{-1}), and LAI_j^{sun} and LAI_j^{sha} are leaf area index for sunlit leaves and shaded leaves, respectively. LAI is total leaf area index that is related to photosynthetic capacity and leaf biomass formation, and these processes are directly affected by atmospheric CO_2 concentration and resource availability of heat, light, water and nutrient. Ω is a PFT specific parameter to represent foliage clumping effect. θ_{ave} is the solar zenith angle.

Stomatal conductance in the model is calculated as a function of photosynthetically active radiation, atmospheric CO_2 concentration, maximum and minimum stomatal conductance and vapor pressure deficit [*Chen et al.*, 2005; *Hijmans et al.*, 2005; *Running and Coughlan*, 1988] using the relation below:

$$g_s = \max \left(g_{max} r_{corr} bf\left(ppdf\right) f\left(T_{min}\right) f\left(vpd\right) f\left(CO_2\right), g_{min}\right) \tag{3a}$$

$$r_{corr} = \left(\frac{T_{day} + 273.15}{293.15}\right)^{1.75} \times \left(\frac{101300}{p}\right) \tag{3b}$$

$$f\left(\text{ppdf}\right) = \frac{\text{ppdf}}{75 + \text{ppdf}} \tag{3c}$$

$$b_i = \begin{cases} 1 & \psi_i > \psi_{\text{open}} \\ \frac{\psi_{\text{open}} - \psi}{\psi_{\text{open}} - \psi_{\text{close}}} & \psi_{\text{close}} \le \psi_i \le \psi_{\text{open}} \\ 0 & \psi_i < \psi_{\text{close}} \end{cases} \tag{3d}$$

$$b = \sum_{i=1}^{10} \left(\text{root}_i \frac{\theta_{\text{sat},i} - \theta_{\text{ice},i}}{\theta_{\text{sat},i}} b_i \right) \tag{3e}$$

$$f\left(T_{\text{min}}\right) = \begin{cases} 1 & T_{\text{min}} > 0°C \\ 1 + 0.125 T_{\text{min}} & -8°C \le T_{\text{min}} \le 0°C \\ 0 & T_{\text{min}} < -8°C \end{cases} \tag{3f}$$

$$f(\text{vpd}) = \begin{cases} 1 & \text{vpd} < \text{vpd}_{\text{open}} \\ \frac{\text{vpd}_{\text{close}} - \text{vpd}}{\text{vpd}_{\text{close}} - \text{vpd}_{\text{open}}} & \text{vpd}_{\text{open}} \le \text{vpd} \le \text{vpd}_{\text{close}} \\ 0 & \text{vpd} > \text{vpd}_{\text{close}} \end{cases} \tag{3g}$$

$$f\left(CO_2\right) = -0.001 CO_2 + 1.35 \tag{3h}$$

Where g_s is the stomatal conductance; r_{corr} is the correction factor of temperature and air pressure on conductance; b is the soil moisture factor; $ppdf$ is the photosynthetic photo flux density (umol m^{-2} s^{-1}); T_{min} is the daily minimum T (°C); vpd is the vapor pressure deficit (pa); CO_2 is the atmospheric CO_2 concentration (ppm); g_{max} and g_{min} are the maximum and minimum stomatal conductance for vapor (m s^{-1}), respectively. p is the air pressure (pa); $\theta_{sat,i}$ is the ith soil layer saturated volumetric water content (mm H$_2$O m^{-2}); $\theta_{ice,i}$ is the volumetric ice content of the ith soil layer (mm H$_2$O m^{-2}); ψ is the water potential (mm H$_2$O); ψ_{open} and ψ_{close} are the water potential under which the stomata fully opens and closes, respectively (mm H$_2$O); vpd_{close} and vpd_{open} are the vapor pressure deficit (vpd) when the leaf stomata is fully closed and open, respectively (Pa).

For the simulation of soil moisture dynamics in different soil layers, the Richards' equation is adopted in DLEM 2.0 [*Oleson et al.*, 2008]. For irrigated cropland, if the estimated transpiration is larger than available soil water, water deficiency is assumed to be replenished by irrigation. The equations for bare-ground in the FAO-56 were revised for soil evaporation simulation. Improvements were made to consider the influence of the vegetation canopy on net radiation and aerodynamic resistance. First, shortwave radiation through canopy is used as the energy source in the Penman–Monteith equation to estimate the potential soil evaporation (PSE). Then, the PSE is adjusted by leaf area according to *Belmans et al.* [1983]:

$$\text{EVAP} = \text{pet}_{\text{PM}} e^{-0.6 \text{LAI}} \tag{4}$$

Where *EVAP* is the soil evaporation; pet_{PM} is the PET estimated with the Penman–Monteith equation, and *LAI* is the average LAI over the land area in each grid.

In this study, we further estimated the effects of direct CO_2 fertilization on terrestrial ET by calculating the "beta" (β) effect. β effect measures the relative strength of changes in terrestrial ET in response to elevated CO_2 concentration as given below:

$$\text{ET}_{CO_2} = \frac{\text{ET}_{\text{clm}+CO_2} - \text{ET}_{\text{clm}}}{CO_{2\text{concentration}} \, (\text{ppm})} \tag{5}$$
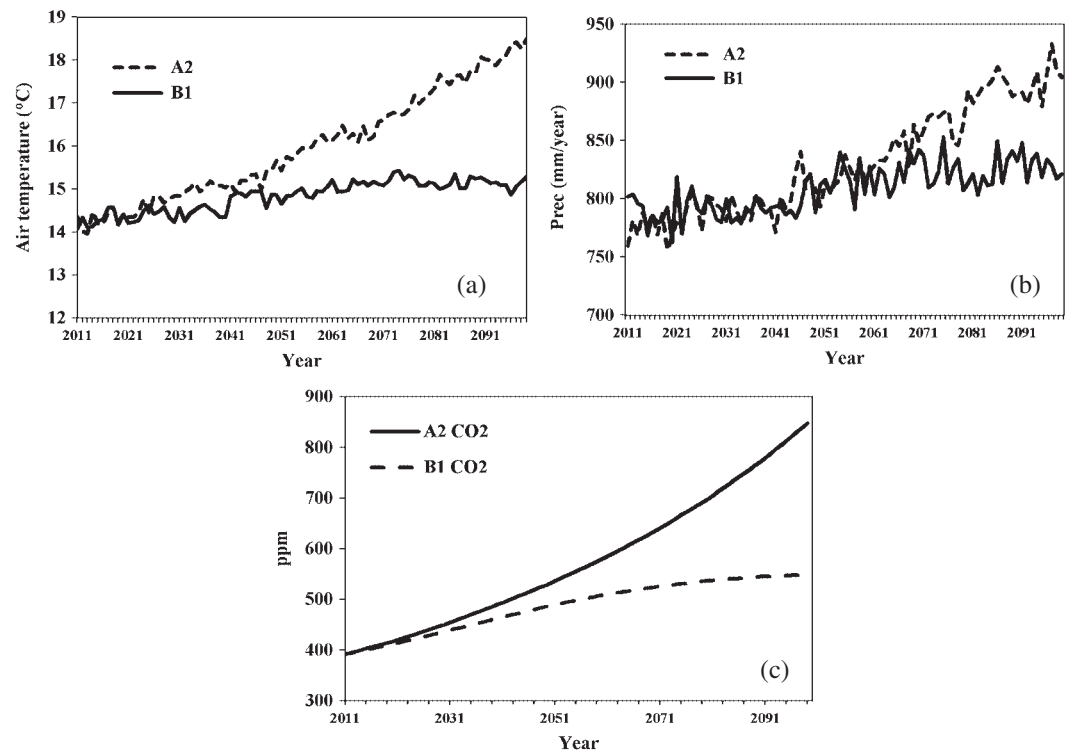
Figure 2. Temporal pattern of input datasets used for driving DLEM based on CRUNCEP analysis during 2010–2099. Temperature change for A2 and B1 (a), precipitation change for A2 and B1 (b) and changes in CO_2 concentration in the A2 and B1 emission scenarios.

2.2. Input Datasets

The datasets for driving the DLEM model include time series of daily climate, annual LULC, nitrogen deposition, O_3, CO_2 concentration, and land management practices (irrigation and nitrogen fertilizer use). In addition, other ancillary data sets such as river network, cropping system information, soil property, and topography maps are used to drive the model to estimate the magnitude of terrestrial ET for the period 2000–2009. Four types of natural vegetation (forests, grassland, shrubland, and wetland) distribution at grid cell levels were generated based on modified SYNMAP land cover products (http://webmap.ornl.gov/wcsdown/wcsdown.jsp?dg_id=10024_1). The cropland and urbanland distribution data were developed by aggregating the 5-min resolution HYDE v3.1 global cropland distribution data [*Klein Goldewijk et al.*, 2011].The half degree daily climate data (including average, maximum, and minimum air temperature, precipitation, relative humidity, and shortwave radiation) were developed based on newly available CRU-NCEP climate forcing data (1901–2010, 6-hour, half degree spatial resolution) for the historical period simulations. Long-term average climate data from 1901 to 1930 were used to represent the initial climate state in 1900.

For the future projection, we adopted projected data on climate (precipitation and temperature) and atmospheric CO_2 concentration from the climate model (CCSM3) under A2 and B1 IPCC emissions scenarios (Figures 2a and 2b and 3a–3d). Data were downloaded from the World Climate Research Programme's Coupled Model Intercomparison Project phase 3 (CMIP3) multi-model dataset (*Meehl et al.* [2007]; www.engr.scu.edu/emaurer/global_data). These data were downscaled using the bias-correction/spatial downscaling method as described by *Maurer et al.* [2009] to a 0.5 degree grid, based on the 1950–1999 gridded observations of *Adam and Lettenmaier* [2003]. The A2 scenario is characterized by continuously increasing population and a regionally oriented economic development, while the B1 scenario is less material intensive in its service and informational economic structure compared to A2 scenario, with emerging clean and resource-efficient technology [*IPCC*, 2007]. For the future projection (2010–2099), we assume that nitrogen deposition, O_3 pollution, and land use/cover remain unchanged since 2010.
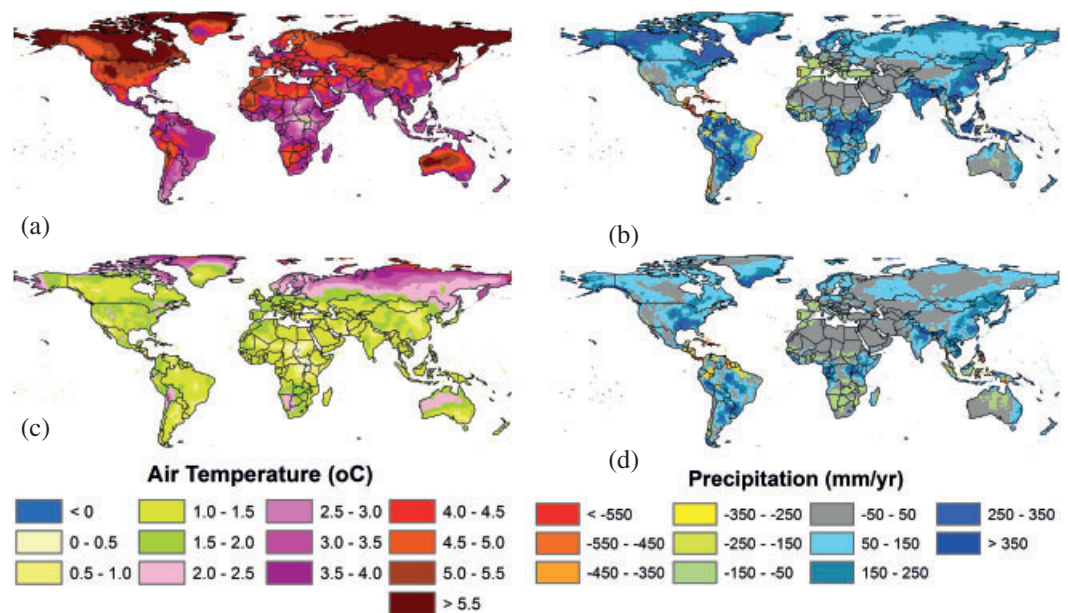
Figure 3. Spatial pattern of change in temperature and precipitation estimated as an average difference between 2099–2090 and 2000–2009: temperature (a) and precipitation (b) under A2 scenario and temperature (c) and precipitation (d) under B1 scenario.

Both temperature and precipitation demonstrate substantial temporal and spatial variations during the lapse of the 21st century (Figures 2a and 2b and 3a–3d). Average temperature in the 2090s would increase by 4.6°C and 1.5°C compared with the 2000s' level under the A2 and B1 scenarios, respectively. Precipitation would increase by 16.9% and 7.5% under A2 and B1 scenarios, respectively, in the 2090s compared with the 2000s. Similarly, atmospheric CO_2 concentration will increase by 114.9% and 44.5% in the 2090s compared to the 2000s under A2 and Bl scenarios, respectively.

2.3. Model Parameterization and Performance Evaluation

The DLEM has been parameterized in various PFTs using long-term observational data across global land surface. The determined parameter values have then been used to validate the model for specific PFTs by comparing it with independent field observations, and regional and continental estimates. In the DLEM 2.0 version, we used parameters related to ecological and plant physiological processes based on previous studies over North America. However, some of the parameters related to ET were recalibrated due to changes in model structure and equations.

In this study, we further evaluated DLEM-simulated terrestrial ET against three independent data sets: (1) flux tower observations at a site level, (2) remote sensing-derived terrestrial ET at global level, and (3) empirically based terrestrial ET derived from network of eddy covariance towers using the model tree ensembles (MTE) approach [*Jung et al.*, 2010] at a global level. We first evaluated DLEM-simulated ET against measured ET data at 21 AmeriFlux sites in the continental U.S. covering multiple ecosystem (Figure 4). DLEM 2.0 ET simulations are close to observational data at most sites in average ET and standard deviations. According to the comparison, we found a significant correlation between model simulation and observation ($R^2 = 0.67$, $p < 0.001$). The comparison suggested that DLEM 2.0 is capable of providing reasonable estimates of ET over a variety of PFTs. In addition, evaluations of DLEM-simulated ET at other eddy covariance sites are available in our previous work [*Tian et al.*, 2010a; *Yang et al.*, 2014].

At a global level, we evaluated spatial pattern in terrestrial ET by comparing DLEM-simulated ET with the MODIS ET product (Figure 5). DLEM-simulated ET shows a tendency of over-prediction when compared to MODIS ET estimates; however, DLEM appropriately captures spatial heterogeneity with higher ET in tropical regions and lower ET in mid- and high-latitude regions. We estimated a global terrestrial ET of about 549 (545–552) mm yr^{-1} that is higher than the MODIS estimate of about 490 (485–495) mm yr^{-1} during
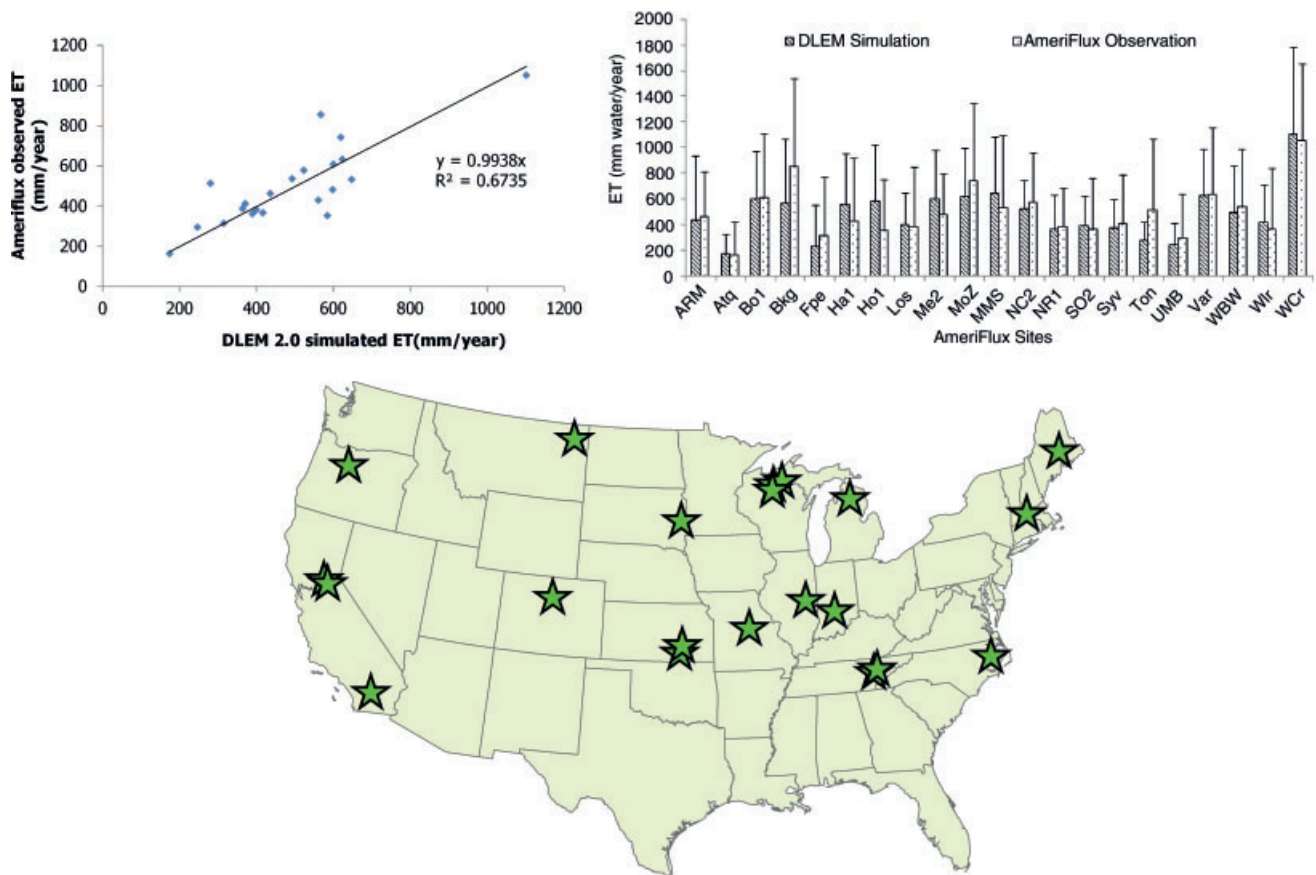
Figure 4. Comparison of DLEM-simulated daily ET with eddy covariance observations at 21 Ameriflux sites in the continental US. Atq: Atqasuk; Bo1: Bondville; Bkg: Brookings; Fpe: Fort Peck; Ha1: Harvard Forest; Ho1: Howland Forest Main; Los: Lost Creek; Me2: Metolius Intermediate Pine; Moz: Missouri Ozark; MMS: Morgan Monroe State Forest; NC2: North Carolina Loblolly Pine; NR1: Niwot Ridge; SO2: Sky Oaks Old; Syv: Sylvania Wilderness Area; Ton: Tonzi Ranch; UMB: UMBS; Var: Vaira Ranch; WBW: Walker Branch; Wlr: Walnut River; WCr: Willow Creek.

2000–2009. We further randomly selected 5000 grids from our global simulation to compare them with MODIS-based ET. Our results show a good correlation between MODIS-estimated and DLEM-simulated ET (y = 0.72x; R^2 = 0.73).

We further compared the DLEM-simulated global terrestrial ET with the MTE approach based on *Jung et al.* [2010] (Figure 6). The MTE uses information from a network of eddy covariance towers (FLUXNET), remote sensing and meteorological observations to estimate the global terrestrial ET at 0.5° spatial resolution, allowing comparison with DLEM results at the same resolution. DLEM captures spatial heterogeneity at a global level with higher ET in low latitude regions and lower ET in mid- and high-latitude regions. DLEM simulated global terrestrial ET of about 549 (545–552) mm yr^{-1} is higher than the MTE estimate of about 481 (473–486) mm yr^{-1} during 2000–2009. However, DLEM-simulated ET shows a good correlation with the MTE ET estimates for 5000 randomly selected grid cells (y = 0.85x; R^2 = 0.88). Discrepancies between our simulation and MODIS/MTE data products are discussed in section 4.1.

2.4. Simulation Protocol and Model Implementation

To project potential changes in global terrestrial ET and quantify the relative contributions of climate and atmospheric CO_2 concentration, we performed four simulation experiments (2 simulations × 2 scenarios). The two scenarios include A2 and B1 climate change scenarios, while the two simulations include: (1) climate change only where climate forcing factors change alone during the study period of 2010–2099 and all other environmental factors, including CO_2 concentration, are kept at the level in year 2010; and (2) climate plus CO_2 where both climate forcing factors and CO_2 change during 2010–2099, and other
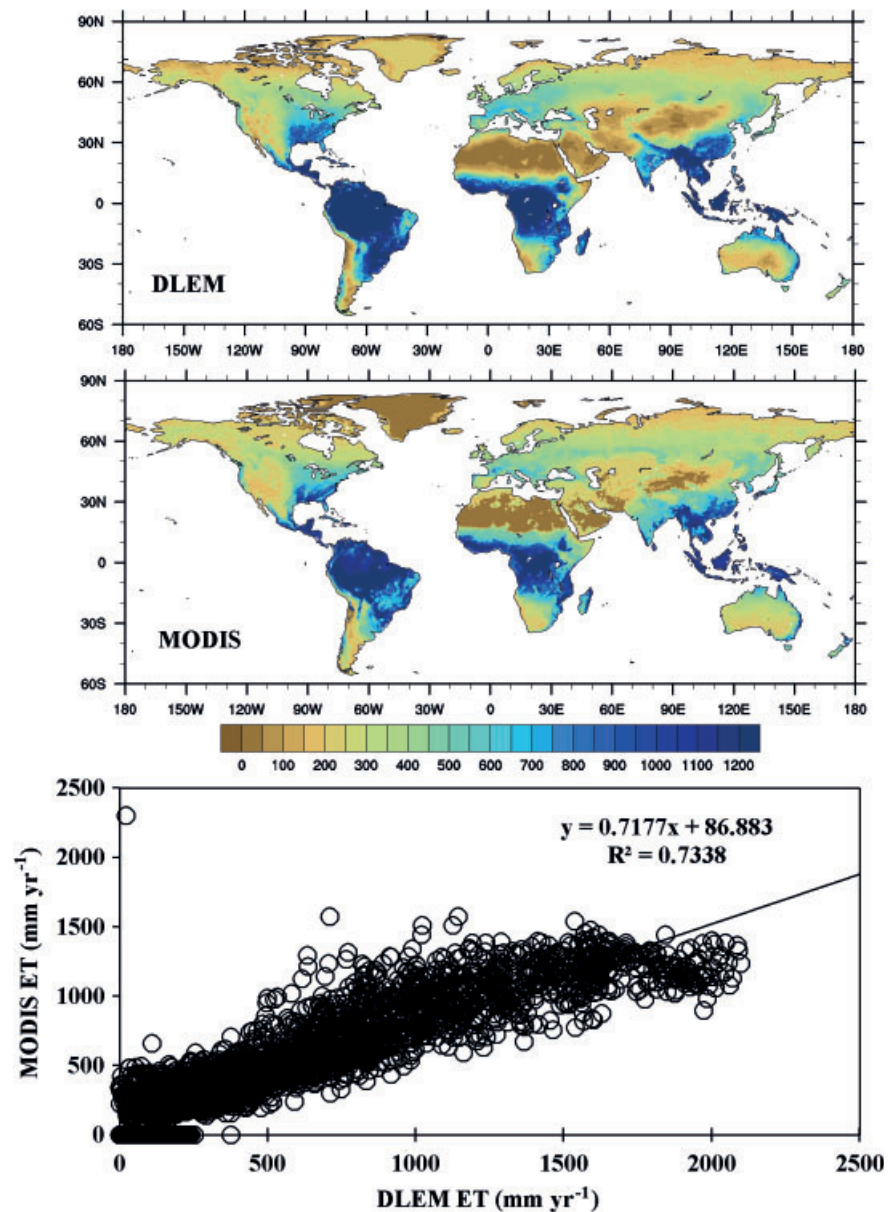
Figure 5. Spatial patterns of DLEM-simulated ET (top), MODIS ET (middle) and comparison of DLEM-simulated versus MODIS ET (bottom) for 5000 randomly selected grids during first decade of the 21st century (2000–2009).

environmental factors including LULC, nitrogen deposition, and tropospheric O_3 are held constant at the 2010 levels during the course of the future projected simulations (2010–2099).

The model runs at a daily time step and follows three important stages: an equilibrium run, a 3000-year spin-up, and a transient run. The equilibrium run is based on long-term average climate data for the period 1901–1930, with 1901 level of atmospheric CO_2 concentration, tropospheric O_3, nitrogen deposition, and potential vegetation map. The baseline (equilibrium) is obtained when year-to-year changes in carbon, nitrogen, and water pools in each grid are less than 0.1 gC m^{-2}, 0.1 mm H_2O, and 0.1 gN m^{-2}, respectively. After the equilibrium run, a 3000-year spin up is carried out to eliminate system fluctuations caused by a shift in simulation from equilibrium to transient mode. Then, a transient simulation is set up driven by a time series of input data sets including climate, atmospheric CO_2, LULC, nitrogen deposition, and tropospheric O_3 in the transient mode.
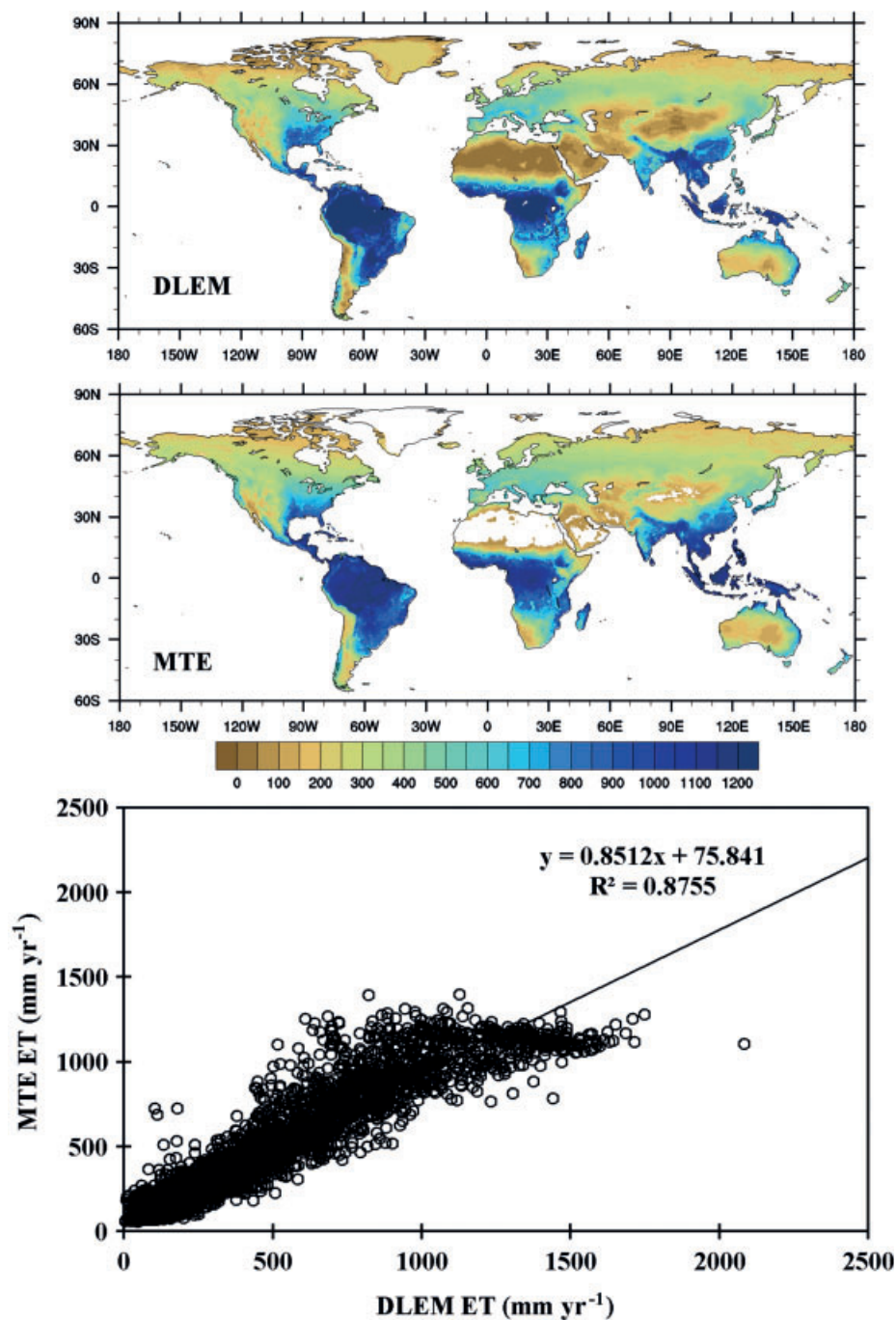
Figure 6. Spatial patterns of DLEM-simulated ET (top), MTE ET (middle) and comparison of DLEM-simulated vs. MTE ET (bottom) for 5000 randomly selected grids during first decade of the 21st century (2000–2009).

3. Results

3.1. Changes in Terrestrial ET Induced by Climate Change and Increasing CO_2 During 2010–2099

3.1.1. Temporal Responses of Terrestrial ET to Climate Change

Our model simulation showed that climate change would result in an overall increase in terrestrial ET by 14% and 4.5% in the 2090s compared to the 2000s under the A2 and B1 scenarios, respectively. Both A2 and B1 climate only scenarios showed an increasing trend in ET throughout the rest of the 21st century
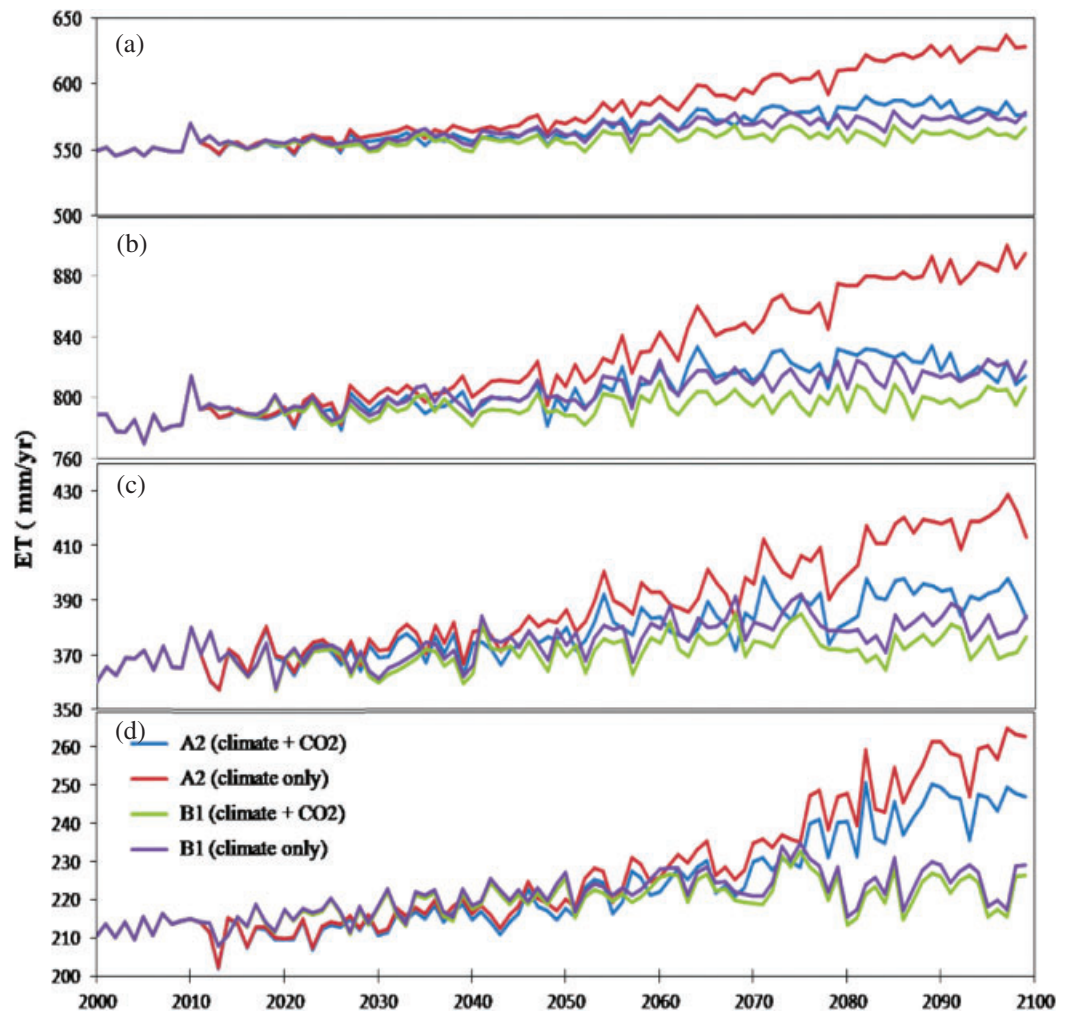
Figure 7. Temporal pattern of change in terrestrial ET: Global (a), low latitude (b), mid-latitude (c) and high latitude (d) as a function of climate and increasing atmospheric CO_2 under A2 and B1 scenarios.

($p < 0.01$) (Figure 7a and Table 1). The increase in terrestrial ET was more prevalent under the A2 scenario than the B1 scenario, primarily due to a substantial increase in air temperature ($p < 0.01$; $R^2 = 0.54$). The A2 and B1 climate only scenarios, would increase terrestrial ET by 9.5 mm decade^{-1} and 2.8 mm decade^{-1}, respectively during the period 2010–2099. Precipitation, in particular, resulted in an overall increase in terrestrial ET under both A2 ($y = 2.0x$, $R^2 = 0.32$) and B1 ($y = 1.2x$; $R^2 = 0.14$) scenarios, but the effect was not significant.

3.1.2. Temporal Responses of Terrestrial ET to Climate Change and Increasing Atmospheric CO_2 Concentration

Climate change and increasing atmospheric CO_2 concentration would result in lower global terrestrial ET than climate change alone under both A2 and B1 scenarios (Figure 7a and Table 1). Both the A2 and B1 scenarios showed an overall increasing trend in terrestrial ET during the rest of the 21st century with the larger increase under the A2 scenario (5.6%) than that under the B1 scenario. The B1 climate plus CO_2 simulation, however, showed a modest increase in terrestrial ET (2.4%) during the 2090s compared to that of the 2000s. The increase in ET was often associated with increasing precipitation ($y = 2.97x$; $R^2 = 0.68$) and surface air temperature ($y = 0.06x$; $R^2 = 0.54$) under the A2 scenario. However, the B1 climate plus CO_2 scenario showed weak correlations between climate factors and ET.

Table 1. Decadal Change in Terrestrial ET Across Global, and Latitudinal (Low-, Mid- and High Latitudes) Level Under A2 and B1 Scenarios for Climate and Climate Plus CO_2 Experiment

		Global ET (mm yr^{-1})		
2000s	549.25			
	A2 (Climate Only)	A2 (Climate +CO_2)	B1(Climate Only)	B1 (Climate + CO_2)
2030s	564.16(2.7%)	558.96(1.8%)	559.41(1.9%)	555.54(1.1%)
2060s	590.93(7.6%)	573.28(4.4%)	571.84(4.1%)	562.71(2.5%)
2090s	626.15(14.0%)	579.96(5.6%)	573.87(4.5%)	562.40(2.4%)
		Low Latitude ET (mm yr^{-1})		
2000s	781.97			
	A2 (Climate Only)	A2 (Climate +CO_2)	B1(Climate Only)	B1 (Climate + CO_2)
2030s	804.60(2.9%)	796.90(1.9%)	799.74(2.3%)	793.94(1.5%)
2060s	843.45(7.9%)	817.02(4.5%)	813.35(4.0%)	799.75(2.3%)
2090s	886.02(13.3%)	816.75(4.4%)	817.46(4.5%)	800.54(2.4%)
		Mid-Latitude ET (mm yr^{-1})		
2000s	366.64			
	A2 (Climate Only)	A2 (Climate +CO_2)	B1(Climate Only)	B1 (Climate + CO_2)
2030s	375.55(2.4%)	372.19(1.5%)	368.42(0.5%)	365.97(−0.2%)
2060s	391.67(6.8%)	380.71(3.8%)	381.46(4.0%)	375.60(2.4%)
2090s	419.35(14.4%)	391.38(6.7%)	381.63(4.1%)	374.11(2.0%)
		High Latitude ET (mm yr^{-1})		
2000s	212.87			
	A2 (Climate Only)	A2 (Climate +CO_2)	B1(Climate Only)	B1 (Climate + CO_2)
2030s	216.50(1.7%)	215.28(1.1%)	219.18(3.0%)	218.37(2.6%)
2060s	229.23(7.7%)	224.83(5.6%)	225.36(5.9%)	223.38(4.9%)
2090s	259.04(21.7%)	245.91(15.5%)	225.00(5.7%)	222.40(4.5%)

3.2. Spatial Patterns of Terrestrial ET Induced by Climate Change and Increasing CO_2 During 2010–2099

3.2.1. Spatial Patterns of Terrestrial ET in Response to Climate Change

Our results showed substantial variations in terrestrial ET along latitudes due to climate change during the rest of the 21st century (Figures 7b–7d and Table 1). The magnitude of terrestrial ET would be highest in low latitude regions (769.6–899.9 mm yr^{-1}), and lowest in high latitude regions (202.0–264.7 mm yr^{-1}). The largest increase in ET (21.7%) occurred under the A2 climate only scenario in high latitude regions. The A2 climate only scenario showed a smaller increase (13.3%) in terrestrial ET in low latitude regions compared to mid- and high-latitude regions. Across all latitudes, the A2 climate only simulation showed an overall increasing trend in terrestrial ET (p < 0.001). The B1 climate only scenario, however, showed a modest increase in terrestrial ET during the 2090s compared to the 2000s across all latitudes. The largest increase in terrestrial ET occurred in high latitude regions (5.7%). The B1 climate only scenario showed a decline in terrestrial ET after the 2060s in high latitude regions, but the mid- and low latitude regions showed a continuous increase in terrestrial ET during the 2010–2099 period.

Our climate only simulations showed an increase in terrestrial ET by 25–75 mm yr^{-1} in the boreal and Arctic regions by the end of 2090s under A2 scenario (Figure 8a). The largest increase (225–275 mm yr^{-1}) in terrestrial ET would occur in the tropical regions of South America and Africa. However, the B1 climate only scenario showed a modest increase (25–75 mm yr^{-1}) in ET across the globe except for parts of Australia and Africa where ET declined by >75mm yr^{-1} (Figure 8c). Australia, in particular, showed
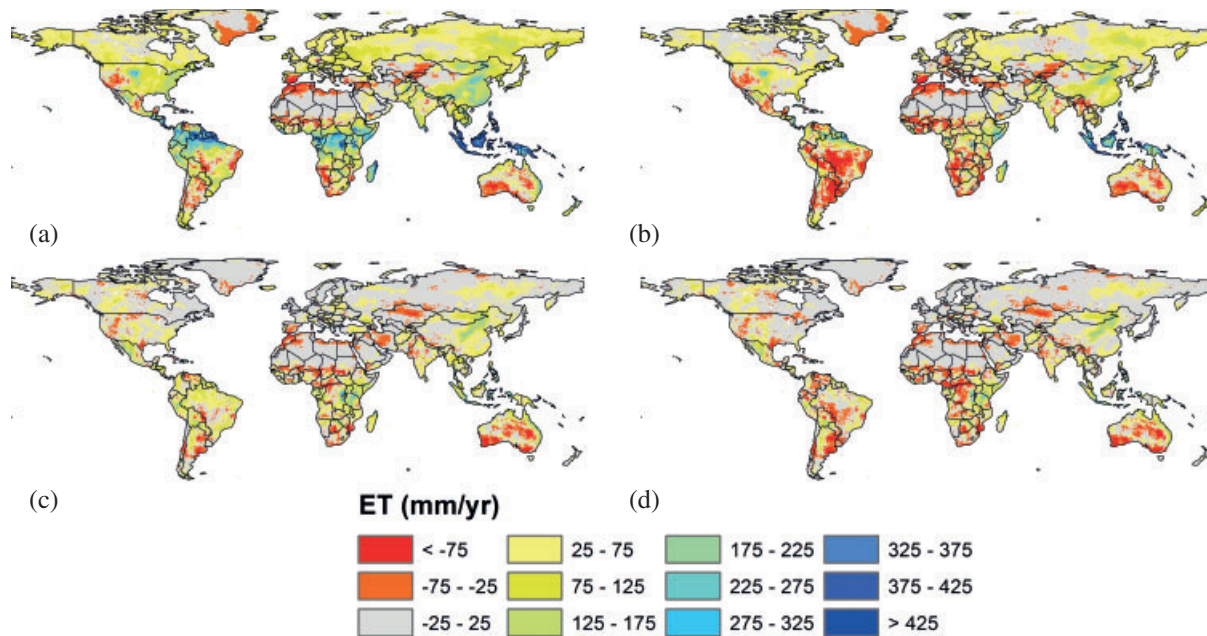
Figure 8. Spatial variation in terrestrial ET due to climate only and climate plus CO_2 experiments estimated as a difference between 2090s and 2000s: climate only (a) and climate plus CO_2 (b) under A2 scenario, and climate only (c) and climate plus CO_2 (d) under B1 scenario.

a declining trend in terrestrial ET under both A2 and B1 scenarios due to limited moisture available for temperature-enhanced ET.

3.2.2. Spatial Patterns of Terrestrial ET Response to Climate Change and Increasing CO_2

The experiment with climate and increasing CO_2 concentration showed substantial difference in the magnitude and temporal pattern of terrestrial ET along the latitudinal gradient. Under the A2 scenario, the combined impact of climate warming and elevated CO_2 on ET would be largest in high latitude regions (33.04 mm yr^{-1}) with an increase of 15.5% by the end of this century, compared to the 2000s' level (Figure 8b and Table 1). However, under the B1 scenario, there will be a modest increase in terrestrial ET by 9.53 mm yr^{-1} in high latitude regions equivalent to an increase of 4.5% for the 2090s compared to the 2000s's level (Figure 8d and Table 1). In mid- and low latitude regions, the A2 scenario showed an increase in terrestrial ET by 6.7% and 4.4% in the 2090s, respectively. Under the B1 scenario, the ET increase in mid- and low latitude regions during the 2090s would be around 2% compared to the 2000s.

3.3. ET Response to Climate Change and Increasing CO_2 for Different Biomes

3.3.1. Biome ET Response to Climate Change

Our results showed large variations in the responses of terrestrial ET across various biomes to future climate change (Table 2). The A2 climate only scenario would result in the largest rate of increase in ET occurring in the boreal needleleaf deciduous forest and tundra by 101.1 and 53.2 mm yr^{-1} equivalent to an increase of 32.7% and 26.6%, respectively. However, the largest magnitude (224.3 mm yr^{-1} or 15.3%) of increase in ET occurred in the tropical broadleaf evergreen forest biome. The tropical broadleaf deciduous forest showed the smallest increase in terrestrial ET (by 8.9%) under the A2 scenario. The B1 scenario, however, showed no substantial increase in ET (only 2–6.2%) across all biomes except for the boreal needleleaf deciduous forest (10.8%). Comparisons of the A2 and B1 climate only scenarios indicated that the A2 scenario would result in a higher ET than the B1 scenario across all biomes. Under the A2 scenario, ET was 46–80% higher across all biomes compared to the B1 climate only scenario, indicating that increasing temperature can substantially increase ET across all biomes.

Table 2. Decadal Mean of Terrestrial ET in the Contemporary Period (2000–2009) and Change in ET Between the 2090s and the 2000s Among Global Plant Functional Types

PFTs	Decadal Mean 2000s (mm yr^{-1})	A2 Net Change (% change) Climate only	A2 Net Change (% change) Climate + CO$_2$	B1 Net Change (% change) Climate only	B1 Net Change (% change) Climate + CO$_2$
Tundra	200.39	53.2 (26.6)	42.6 (21.3)	10.8 (5.4)	8.6 (4.3)
BNEF	316.57	45.4 (14.3)	27.9 (8.8)	15.2 (4.8)	11.1 (3.5)
BNDF	309.13	101.1 (32.7)	75.3 (24.3)	33.5 (10.8)	27.5 (8.9)
TBDF	598.79	98.0 (16.4)	26.9 (4.5)	28.9 (4.8)	9.1 (1.5)
TBEF	981.28	154.7 (15.8)	45.9 (4.7)	34.5 (3.5)	5.4 (0.5)
TNEF	443.55	75.1 (16.9)	35.6 (8.0)	20.4 (4.6)	10.0 (2.2)
TrBDF	1000.41	89.2 (8.9)	−3.9 (0.4)	48.3 (4.8)	24.6 (2.4)
TrBEF	1465.27	224.3 (15.3)	75.4 (5.1)	62.4 (4.3)	24.3 (1.7)
Deciduous Shrub	313.23	49.2 (15.7)	24.3 (7.8)	12.7 (4.1)	6.9 (2.2)
Evergreen Shrub	620.10	61.7 (9.9)	15.5 (2.5)	29.0 (4.7)	19.1 (3.1)
C3 grass	358.61	50.0 (13.9)	27.8 (7.8)	20.8 (5.8)	15.7 (4.4)
Herbaceous wetland	314.76	55.3 (17.6)	21.3 (6.8)	19.6 (6.2)	12.4 (4.0)
Woody wetland	987.59	108.4 (11.0)	7.7 (0.8)	28.8 (2.9)	4.2 (0.4)
Cropland	620.87	83.7 (13.5)	38.9 (6.3)	26.3 (4.2)	14.5 (2.3)

Numbers in parenthesis represent percentage change between the 2090s and the 2000s.

3.3.2. Biome ET Responses to Climate Change and Increasing CO$_2$ Concentration During 2010–2099

Climate change coupled with increasing atmospheric CO$_2$ concentration would lead to an overall increase in ET across almost all biomes under both the A2 and B1 scenarios (Table 2). For the A2 scenario, the largest increase in ET would occur in the tundra (21.3%) and the boreal needleleaf deciduous forest (24.3%), while the smallest increase would occur in woody wetlands (0.8%). The ET declined by 0.4% for tropical broadleaf deciduous forest under the A2 scenario. The B1 scenario with climate change and increasing CO$_2$ showed an overall increase in ET across all biomes in the range of 0.4–8.9%. In general, increased CO$_2$ coupled with climate change would reduce the increase in ET across all biomes compared to the climate only simulation, primarily because increasing CO$_2$ results in a partial closure of stomata that would reduce the loss of water from leaves.

3.4. CO$_2$ Fertilization Effects on Terrestrial ET

Our results indicate that the strength of the CO$_2$ fertilization effect would determine the magnitude of global terrestrial ET during the 21st century. Terrestrial ET during the 2090s would decrease due to increasing atmospheric CO$_2$ concentration across the globe with substantial spatial variability (Figure 9). In low latitude regions under the A2 scenario, increasing atmospheric CO$_2$ concentration would reduce terrestrial ET by over 170 mm yr^{-1} in the northern regions of South America, central Africa, and Southeast Asia. In the B1 scenario, however, CO$_2$ fertilization leads to a modest decline (30–50 mm yr^{-1}) in terrestrial ET across South America and Central Africa during the 2090s. During the rest of the 21st century, the CO$_2$ fertilization would result in a net decline in global terrestrial ET by 0.55 mm yr^{-1}, and 0.14 mm yr^{-1} equivalent to a decrease of 8.8% and 2.2% compared to the contemporary period under A2 and B1 scenarios, respectively.

We further calculated the beta "β" effect to quantify the effects of increasing atmospheric CO$_2$ concentration on terrestrial ET at global and latitudinal levels (Figure 10). Our results showed that the effect of direct CO$_2$ fertilization would be 56.8 μm m^{-2} yr^{-1}/CO$_2$ (ppm) under the A2 scenario during the 2090s implying that 1 ppm of CO$_2$ would result in saving about 56.8 μm m^{-2} yr^{-1} of water. The effect of direct CO$_2$ fertilization, however, would be lower under the B1 scenario due to a lower concentration of atmospheric CO$_2$ compared to the A2 scenario. In addition, there was substantial variation in terrestrial ET due to direct CO$_2$
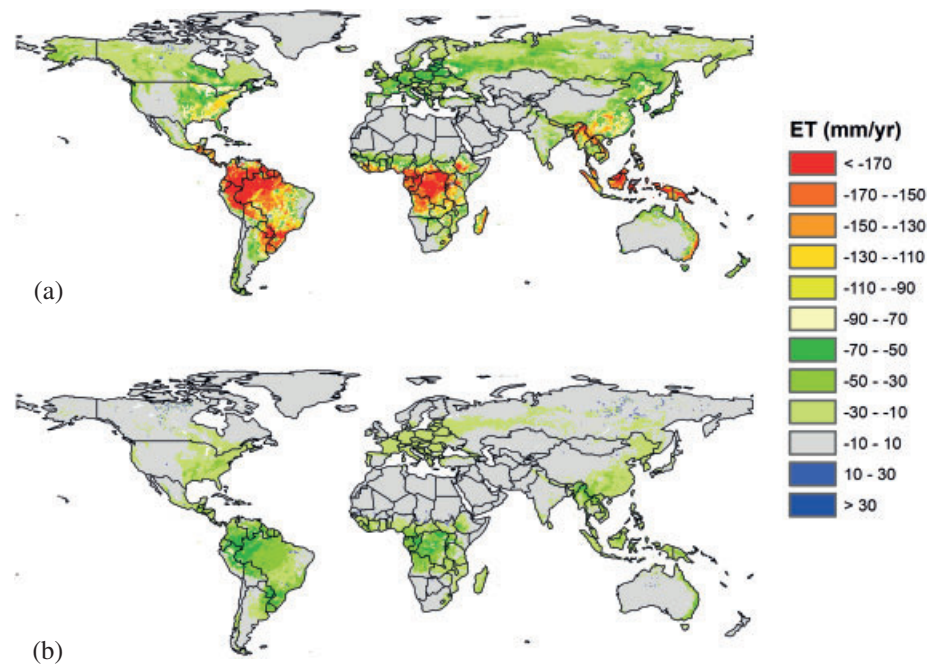
Figure 9. Contribution of increasing atmospheric CO_2 concentration to terrestrial ET during the 2090s calculated as a difference between climate plus CO_2 and climate only experiment: A2 scenario (a) and B1 scenario (b).

fertilization across latitudinal regions. The β effect would be highest in low latitude regions (85.15 μm m^{-2} yr^{-1}/CO$_2$ [ppm]) while lowest in high latitude (16.15 μm m^{-2} yr^{-1}/CO$_2$ [ppm]) regions under the A2 scenario. The B1 scenario, however, showed a substantially lower decline in ET due to direct CO_2 fertilization compared to the A1 scenario.

4. Discussion

4.1. Comparison of DLEM-Simulated Baseline (2000–2009) Terrestrial ET with Previous Studies

The DLEM-based estimates of global terrestrial ET are comparable with previous estimation based on remote sensing and other ecosystem models (Table 3). We estimate a mean annual global terrestrial ET of 74.69 × 10^3 km^3 H$_2$0 yr^{-1} (549.24 mm yr^{-1}) for the period from 2000 to 2009, which falls within the model range of 58–85 × 10^3 km^3 H$_2$0 yr^{-1} estimated by the Global Soil Wetness Project 2 [*Dirmeyer et al.*, 2006]. However, *Jung et al.* [2010], in a recent study, estimated a global terrestrial ET of about 65 × 10^3 km^3 yr^{-1}, which is much lower than the DLEM-simulated terrestrial ET. In general, DLEM-simulated ET lies at the higher end of terrestrial ET estimates based on remote sensing and other ecosystem models. Our results (549.24 mm yr^{-1}) match well with *Zhang et al.* [2010] and *Zeng et al.* [2012] reporting a global terrestrial ET of about 539.3 and 602 (558–650) mm yr^{-1}, respectively, but show a tendency for over-estimation when compared to other studies based on remote sensing and water balance models [*Jung et al.*, 2010; *Yan et al.*, 2012]. The discrepancy between our simulated results and other estimates are due to limitations associated with ET measurements across broad temporal and spatial scales, including the lack of accurate observations, accuracy, and physical interpretation of different surface variables retrieved from satellite data, and parameterization of land surface fluxes at different scales.

In recent years, ET estimation at regional and global scale is based on a combination of the eddy covariance technique, remote sensing, and process-based models [*Cleugh et al.*, 2007; *Fisher et al.*, 2008; *Mu et al.*, 2007; *Vinukollu et al.*, 2011; *Zhang et al.*, 2010]. Field measurements of ET rely on eddy covariance techniques that provide direct estimates of ET, but are subject to several sources of uncertainty [*Baldocchi*, 2003; *Drexler et al.*, 2004]. In flux tower measurements, natural vegetation is often less than homogenous both vertically and horizontally, so that the flux measurement may not be homogenous over the area of interest. Additionally, the sum of latent and sensible heat fluxes must be equal to the total incident
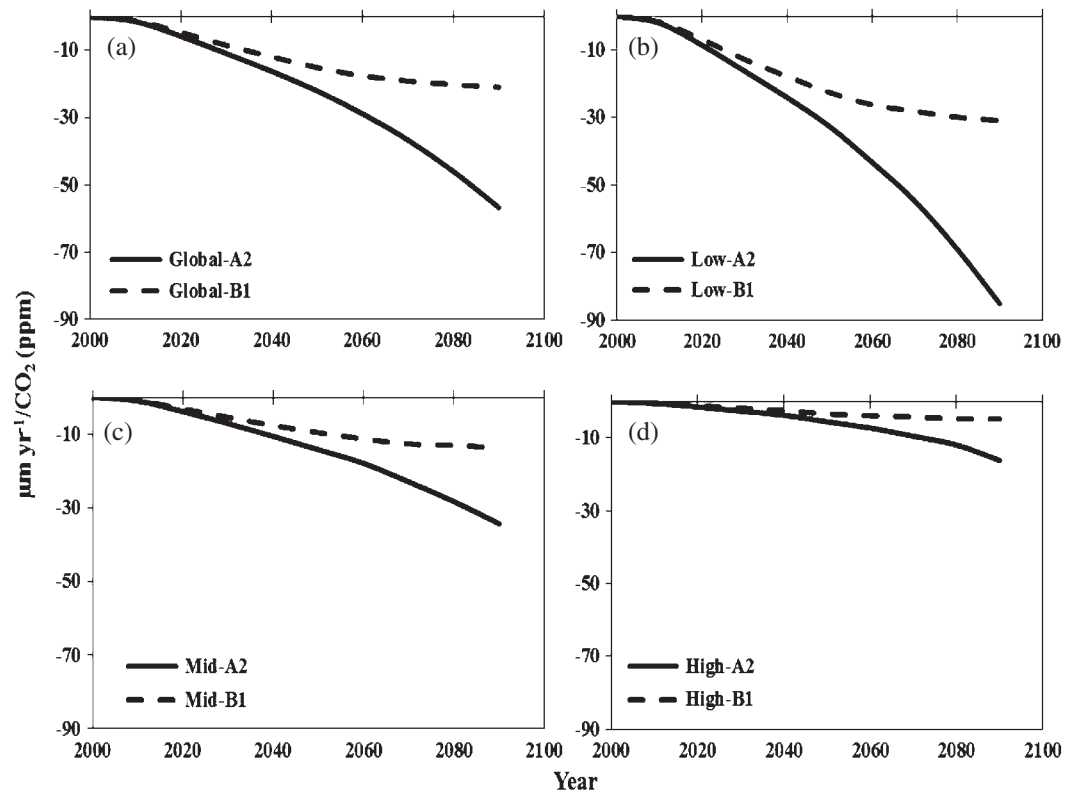
Figure 10. The effect of CO_2 fertilization on terrestrial NPP across the globe (a), low latitude (b), mid-latitude (c), and high latitude (d) under A2 and B1 scenarios. For each unit of CO_2 (ppm), the A2 scenario show a net decline in terrestrial ET (μm yr^{-1} H$_2$o) compared to B1 scenario.

radiation over the area of interest, but an energy balance closure problem is well evident in flux tower measurements [*Li et al.*, 2005].

Similarly, remote sensing-based products used to evaluate the uncertainties in radiation and meteoro-logical forcing data suggest an uncertainty estimate of 30 Wm^{-2} in net radiation when compared among different models which translates to a difference in ET of about 0.26 mm day^{-1} [*Ferguson et al.*, 2010]. The use of the remotely sensed vegetation index (VI) to estimate ET [*Allen et al.*, 2007; *Yang et al.*, 2006] has also gained attention, though these methods rely on foliage density as the main independent variable and do not adequately account for direct evaporation from soil or leaves following a rainfall event [*Glenn et al.*, 2007]. *Liou and Kar* [2014], in a recent study, found several issues associated with ET retrieval from remote sensing approach. Most of these issues are associated with uncertainties related to estimation of surface temperature and solar parameters, limited satellite coverage, estimation of land surface variables such as LAI, vegetative coverage, plant height etc, and inconsistencies among remote sensing ET models due to different land surface characterization.

Another method of ET estimation, FLUXNET-MTE uses the machine learning technique, MTE to upscale water fluxes to a global scale [*Jung et al.*, 2010]. The FLUXNET-MTE provides monthly to annual ET estimates at 0.5° × 0.5° spatial resolution during 1982–2010, allowing comparison with DLEM results for the contemporary period (2000–2009). MTE ET estimates are based on up-scaling local eddy covariance flux measurements from global FLUXNET network, through integration with satellite based FPAR and climate data. However, FLUXNET-MTE does not explicitly take into account environmental factors such as rising atmospheric CO_2 concentration, nitrogen deposition, and LULC [*Shi et al.*, 2013]. Previous studies report that the effect of elevated atmospheric CO_2 concentration is particularly important in determining the amount of water evaporated from the terrestrial surface [*Gedney et al.*, 2006; *Piao et al.*, 2007]. Other factors such as LULC [*Piao et al.*, 2007; *Shi et al.*, 2011] and nitrogen limitation [*Felzer et al.*, 2009] may con-trol the water balance of terrestrial ecosystems. In addition to these shortcomings, it is important to note

Table 3. Comparison of DLEM-Simulated ET With Previous Studies Based on Eddy Covariance Techniques, Remote Sensing Estimates and Process-Based Models

S. No.	Methods	Time Period	Estimated ET	References
1	Remote sensing and meteorological observation, machine learning approach	1982-2008	478 mm yr^{-1} (65 × 10^3 km^3 yr^{-1})	*Jung et al.* [2010]
2	Review and Synthesis	NA	482 mm yr^{-1} (65.5 × 10^3 km^3 yr^{-1})	*Oki and Kanae* [2006]
3	15 Model Simulation, Global Soil Wetness Project 2	1986–1995	(58–85 × 10^3 km^{3}yr^{-1})	*Dirmeyer et al.* [2006]
4	MODIS Improved Algorithm (only vegetated surface)	2000–2006	461.8 mm yr^{-1} (62.8 × 10^3 km^3 yr^{-1})	*Mu et al.* [2011]
5	MODIS Old Algorithm (only vegetated surface)	2000–2006	45.8 × 10^3 km^3 yr^{-1}	*Mu et al.* [2007]
6	NDVI, Penman–Monteith and Priestley–Taylor	1983–2006	539.3 mm yr^{-1} (79.8 × 10^3 km^3 yr^{-1})	*Zhang et al.* [2010]
7	Water Balance equation, NDVI and Meteorological Data	1982–2009	602 mm yr^{-1} (89 × 10^3 km^3 yr^{-1})	*Zeng et al.* [2012]
8	MODIS and Global Meteorological Data	2000–2003	417 mm yr^{-1} (61.7 × 10^3 km^3 yr^{-1})	*Yuan et al.* [2010]
9	Satellite, AVHHR and Fluxnet	1986–1993	444 mm yr^{-1} (65.7× 10^3 km^3 yr^{-1})	*Fisher et al.* [2008]
10	Penman–Monteith and Water Balance Model	1984–1998	429.4 mm yr^{-1} 58.4× 10^3 km^3 yr^{-1}	*Yan et al.* [2012]
11	Process-based model (DLEM)	2000–2009	549.2 mm yr^{-1} (74.7 × 10^3 km^3 yr^{-1})	This study

that FLUXNET-MTE itself is a modeled product based on a combination of eddy covariance up-scaling and remote sensing data. Therefore, it should not be viewed as ground-truth as there are several uncertainties associated with eddy covariance flux measurements and remote sensing approach.

Likewise, ecosystem models are also subjected to large sources of uncertainty, owing to complex parameterization and the inaccuracy of input data used to drive ecosystem models. DLEM-simulated ET is based on the Penman–Monteith algorithm, which uses leaf area index (LAI) and other empirically derived parameters to estimate global terrestrial ET. This algorithm relies on stomatal conductance parameters based on environmental controls, but such an approach can induce large uncertainty due to the sensitivity of sensible and latent heat fluxes to slight differences in input data such as surface temperature. For example, *Mu et al.* [2007] relied on the Penman–Monteith algorithm developed by *Cleugh et al.* [2007] introducing a stomatal conductance parameterization based on environmental controls, but found several problems associated with estimation of day and night time ET, soil heat flux, stomatal conductance, aerodynamics, and boundary layer resistance [*Mu et al.*, 2011]. Thus, the differences between DLEM-simulated ET and previous studies based on the eddy covariance technique, remote sensing algorithm, and process-based models, might be caused by the inaccuracy of input data in process-based models, uncertainties in radiation and meteorological forcing data in remote sensing algorithm, and the energy closure problem and up-scaling issues associated with eddy covariance techniques.

4.2. Climate Change Impacts on Global Terrestrial ET in the 21st Century

Most future projections show increasing global mean temperature and precipitation during the period 2010–2099 [*IPCC*, 2007]. Climate change has direct effects on hydrological processes [*Liu et al.*, 2008]. Our analysis of the effect of climate on terrestrial ET suggested that climate variability accounted for 91.3% of the inter-annual variation in ET. Correlations between specific climatic factors (precipitation and temperature) indicate that both precipitation (R^2 = 0.83, $p < 0.001$) and temperature (R^2 = 0.81, $p < 0.001$) have significant positive correlations with ET, suggesting that either precipitation or temperature could change ET by affecting AET or PET. An insufficient water supply could be a limiting factor at high temperatures [*Mohan and Arumugam*, 1996]. For example, the maximum temperature during the study period appeared in the 2090s, but it would not induce an extremely high ET during this period, which indicates other factors, such as precipitation, may limit ET. In areas that received low precipitation, ET demonstrated a negative response to temperature increase and vice versa. For example, declines in ET in Australia under the climate only scenario (Figure 7c and 8a) coincide with either declining or no change in precipitation

suggesting the dominant role of insufficient moisture supply [*Jung et al.*, 2010] for ET in these regions. This decline in terrestrial ET may be attributable to the effect of decreasing soil moisture, especially in South America, Africa, and Australia [*Jung et al.*, 2010], or the effect of increased cloudiness [*Dai and Trenberth*, 1999] that could result in a decreased diurnal temperature range.

4.3. Atmospheric CO_2 Effect on ET and Its Interaction with Climate Change

Our analysis showed that increasing CO_2 concentration would determine the magnitude of terrestrial ET during the 21st century. Over the period 2010–2099, DLEM-simulation showed a declining trend in terrestrial ET due to increasing atmospheric CO_2 (Figure 9, 10). Increasing CO_2 concentration would decrease ET by 50 mm yr^{-1} and 10 mm yr^{-1} by the 2090s under the A2 and B1 scenarios, respectively. In addition, our results indicate that the response of terrestrial ET would vary spatially across the globe with the largest reduction in terrestrial ET in low latitude regions and the smallest reduction in high latitude regions. The decrease in ET in response to increasing CO_2 concentration is consistent with chamber experiments that have reported decreased ET under elevated CO_2 concentration [*Kergoat et al.*, 2002; *Rosolem et al.*, 2010]. However, the positive and negative plant transpiration responses to future CO_2 levels should be both considered when interpreting the results of this study.

Two processes are primarily involved in determining the effect of increasing CO_2 on terrestrial ET: (1) reduction in stomatal aperture and (2) increased leaf biomass production. As future climate is projected to demonstrate dramatic spatial and temporal variability, there is much uncertainty on how ET would respond to changes in precipitation and temperature as well as affect global water cycles [*Chattopadhyay and Hulme*, 1997]. First, increasing atmospheric CO_2 concentration indicate reductions in stomatal aperture, resulting in an overall reduction in canopy ET [*Lockwood*, 1995]. Second, although plant transpiration was found to decline with elevated CO_2 due to reductions in stomatal conductance, this effect can be mitigated by the increasing LAI under high CO_2 concentration [*Betts et al.*, 1997; *Kergoat et al.*, 2002]. *Gedney et al.* [2006] reported the suppression of plant transpiration due to CO_2-induced stomatal closure, and resulted in increased runoff at a continental scale. In a similar study, *Betts et al.* [2007] found an increase in continental runoff by 6% relative to pre-industrial levels due to the physiological effect of double CO_2 concentration on plant transpiration. DLEM-simulated reduction in transpiration supports these previous findings, which report increased runoff due to reduction in plant transpiration. However, the impacts of these two counteracting mechanisms on terrestrial ET over large areas need to be investigated as atmospheric CO_2 elevation continues.

Our results further indicate that climate change and its interaction with increasing CO_2 would have a substantial effect on terrestrial ET through reduction in stomatal conductance. For example, in low latitude regions moisture stress associated with increasing temperatures resulted in the largest decline in terrestrial ET under increasing atmospheric CO_2 concentration. The CO_2 fertilization would result in higher CO_2 assimilation; however, it also reduced ET through reduction in stomatal conductance in plants [*Field et al.*, 1995; *Porporato et al.*, 2001]. The concurrent effect of soil moisture limitations [*Felzer et al.*, 2011] and elevated CO_2 on terrestrial ET should be considered while analyzing our results because these mechanisms counteract each other in determining terrestrial ET across the globe.

4.4. The Ratio of ET to Precipitation: Implication for Water Security

ET is a key factor that links the global energy and water cycles. Accurate records of where water availability will be threatened would be critical to the development of adaptation strategies under future climate change scenarios. Global climate change is expected to alter precipitation pattern and terrestrial ET substantially [*Oki and Kanae*, 2006] which could affect the renewable freshwater resources. Terrestrial ET returns about 60% of precipitation to the atmosphere and is considered a most significant component of the hydrologic budget [*Oki and Kanae*, 2006], with important implications for ecosystem services such as fresh water availability and regional climate characteristics [*Seneviratne et al.*, 2006] such as heat waves and climate extremes. A measure of the ratio of evapotranspiration and precipitation (ET/PPT) across the globe would give us an indication about the locations where freshwater resources would be limited in the future. We found that the ET/PPT during the 2090s would be higher in the drylands across the globe (Figure 11). In general, high ET/PPT was found across Africa where ET/PPT exceeded 1.0 under both the A2 and B1 scenarios during the 2090s. The higher ET/PPT is primarily determined by either decrease in precipitation or increase in ET. Under A2 scenario, temperature increases of 16% (approximately 4.6°C) at the
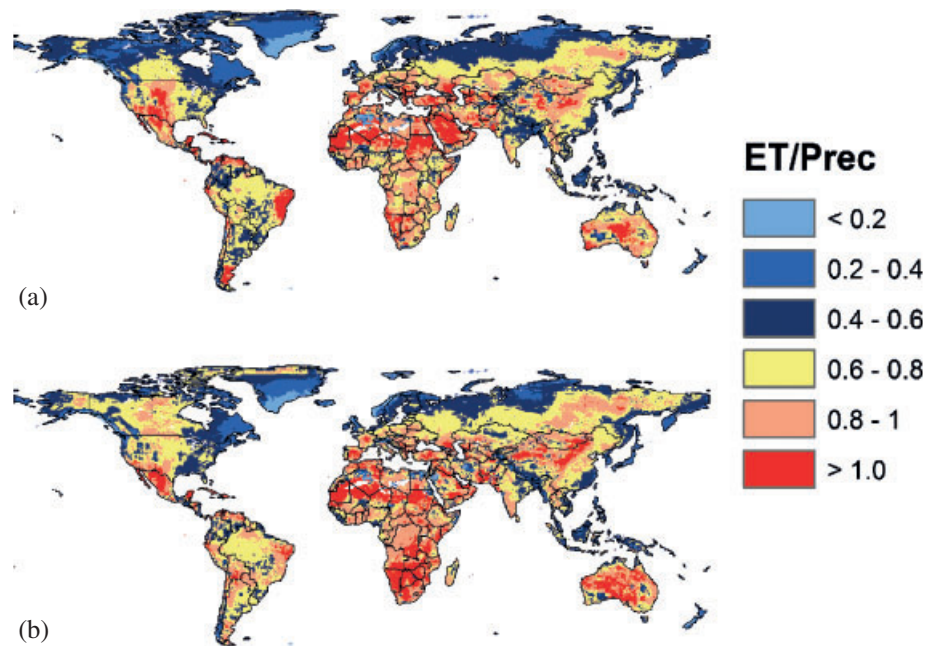
Figure 11. The ratio of evapotranspiration to total precipitation as a measure of potential evaporative demand and moisture supply under A2 (a) and B1 scenario (b).

end of 21st century would result in higher potential atmospheric demand of water leading to an increase in ET/PPT. In contrast, although the B1 scenario shows an increasing trend in precipitation (6%), regions such as southern Africa and parts of Australia would experience a decrease in precipitation (Figure 3d). The low amount of precipitation in these regions would result in a higher ET/PPT. Therefore, changes in precipitation pattern under the B1 scenario and larger increase in air temperature under the A2 scenario would substantially affect freshwater availability in the future.

Our results suggest that arid and semi-arid environments would experience the largest increase in ET/PPT, where water is already a scarce resource [*Jackson et al.*, 2009]. For example, higher ET/PPT is observed across Africa under both the A2 and B1 scenario at the end of 21st century, where at least 44% of the population does not currently have access to clean, reliable water supplies [*WHO/UNICEF*, 2003]. Continued population growth across Africa would cause water consumption levels to increase resulting in acute water scarcity in these regions. Additionally, in most of the mid and low latitude regions ET/PPT indicates that ET would be almost 80% of the total precipitation at the end of 21st century which is higher than the current level of ET that returns 60% of the precipitation to the atmosphere. Maintaining a balance between ET and precipitation is critical to ensure a continuous supply of freshwater resources in the coming decades. To meet the challenge of water scarcity across the globe in a warming world would require both development and the exploitation of new water supplies and comprehensive policies that encourages efficient use of existing resources.

4.5. Uncertainties and Future Research Needs

Although model performance evaluation showed that the DLEM 2.0 had reasonable representations of ET over different PFTs, the following uncertainties should be considered in the interpretation of the model projection of future global ET. Uncertainties in our estimation on water fluxes are mainly derived from several sources including input datasets, model structure, and simplification of some hydrological processes. As we discussed previously, climate is the primary factor controlling terrestrial ET, so the accuracy of climate data is the key to reducing uncertainty in terrestrial ET estimation. In this study, we used future climate projections from only one global climate model. Future assessment of climate change impact on ET needs to make use of multi-model ensembles of projections of future climate change. Besides, land use change is expected to occur at a faster pace and over broader spatial scales, and also nitrogen deposition

and tropospheric O_3 levels are expected to increase in a more polluted world, which would affect future changes in terrestrial ET but not considered in this study.

5. Summary and Conclusions

The DLEM simulations estimate a mean global terrestrial ET of about 549 mm yr^{-1} during 2000–2009 resulting from multiple environmental changes including climate, elevated CO_2, nitrogen deposition, tropospheric O_3, and LULC. During the rest of the 21st century, climate change would result in an overall increase in ET by 14% and 4.5% in the 2090s compared to the 2000s under the A2 and B1 scenarios, respectively. Climate change coupled with increasing atmospheric CO_2 concentration would result in an increase in ET by 5.6% and 2.4% during the 2090s compared to that of the 2000s. Across latitudes, the largest increase (21.7%) in ET would occur in high latitude regions. Similarly, boreal needleleaf deciduous forest and tundra experienced the largest increase in ET of 32.7% and 26.6%, respectively.

Our results further show that arid- and semi-arid environments would experience the largest increase in ET/PPT, where at least 44% of the population does not currently have access to clean water supplies [*WHO/UNICEF*, 2003]. Additionally, compared to the current global ET that returns 60% of the water from terrestrial biosphere to the atmosphere, our projection shows that almost 80% of the water would be returned to the atmosphere by the end of the 21st century. Therefore, maintaining a balance between ET and precipitation is critical to ensure a continuous supply of freshwater during the 21st century.

References

Adam, J. C., and D. P. Lettenmaier (2003), Adjustment of global gridded precipitation for systematic bias, *J. Geophys. Res.: Atmos.*, *108*(D9), 1–15, doi:10.1029/2002JD002499.

Allen, L. (1991), Effects of increasing carbon dioxide levels and climate change on plant growth, evapotranspiration, and water resources, in *Managing Water Resources in the West Under Conditions of Climate Uncertainty*, edited by National Research Council, pp. 101–147, National Academy Press, Washington, D. C.

Allen, R. G., L. S. Pereira, D. Raes, and M. Smith (1998), *Crop evapotranspiration-Guidelines for computing crop water requirements-FAO Irrigation and drainage paper 56*, vol. 300, pp. 6541 , FAO, Rome.

Allen, R. G., M. Tasumi, and R. Trezza (2007), Satellite-based energy balance for mapping evapotranspiration with internalized calibration (METRIC)—Model, *J. Irrig. Drain. Eng.*, *133*(4), 380–394.

Alton, P., R. Fisher, S. Los, and M. Williams (2009), Simulations of global evapotranspiration using semiempirical and mechanistic schemes of plant hydrology, *Global Biogeochem. Cycles*, *23*(4), 1–12, doi:10.1029/2009GB003540.

Arnell, N. W. (1999), Climate change and global water resources, *Global Environ. Change*, *9*, S31–S49, doi:10.1016/S0959-3780(99)00017-5.

Baker, J., L. Allen, K. Boote, P. Jones, and J. Jones (1990), Rice photosynthesis and evapotranspiration in subambient, ambient, and superambient carbon dioxide concentrations, *Agron. J.*, *82*(4), 834–840.

Baldocchi, D. D. (2003), Assessing the eddy covariance technique for evaluating carbon dioxide exchange rates of ecosystems: Past, present and future, *Global Change Biol.*, *9*(4), 479–492, doi:10.1046/j.1365-2486.2003.00629.x.

Belmans, C., J. Wesseling, and R. Feddes (1983), Simulation model of the water balance of a cropped soil: SWATRE, *J. Hydrol.*, *63*(3), 271–286.

Betts, R. A., P. M. Cox, S. E. Lee, and F. I. Woodward (1997), Contrasting physiological and structural vegetation feedbacks in climate change simulations, *Nature*, *387*, 796–799.

Betts, R. A., O. Boucher, M. Collins, P. M. Cox, P. D. Falloon, N. Gedney, D. L. Hemming, C. Huntingford, C. D. Jones, and D. M. Sexton (2007), Projected increase in continental runoff due to plant responses to increasing carbon dioxide, *Nature*, *448*(7157), 1037–1041, doi:10.1038/nature06045.

Cao, L., G. Bala, K. Caldeira, R. Nemani, and G. Ban-Weiss (2010), Importance of carbon dioxide physiological forcing to future climate change, *Proc. Natl. Acad. Sci. U. S. A.*, *107*(21), 9513.

Chattopadhyay, N., and M. Hulme (1997), Evaporation and potential evapotranspiration in India under conditions of recent and future climate change, *Agric. For. Meteorol.*, *87*(1), 55–73.

Chen, J. M., X. Chen, W. Ju, and X. Geng (2005), Distributed hydrological model for mapping evapotranspiration using remote sensing inputs, *J. Hydrol.*, *305*(1), 15–39.

Cleugh, H. A., R. Leuning, Q. Mu, and S. W. Running (2007), Regional evaporation estimates from flux tower and MODIS satellite data, *Remote Sens. Environ.*, *106*(3), 285–304, doi:10.1016/j.rse.2006.07.007.

Dai, A., and K. E. Trenberth (1999), Effects of clouds, soil moisture, precipitation, and water vapor on diurnal temperature range, *J. Clim.*, *12*(8), 2451–2473.

Dirmeyer, P. A., X. Gao, M. Zhao, Z. Guo, T. Oki, and N. Hanasaki (2006), GSWP-2: Multimodel analysis and implications for our perception of the land surface, *Bull. Am. Meteorol. Soc.*, *87*(10), 1381–1397.

Drexler, J. Z., R. L. Snyder, D. Spano, U. Paw, and K. Tha (2004), A review of models and micrometeorological methods used to estimate wetland evapotranspiration, *Hydrol. Processes*, *18*(11), 2071–2101.

Durack, P. J., S. E. Wijffels, and R. J. Matear (2012), Ocean salinities reveal strong global water cycle intensification during 1950 to 2000, *Science*, *336*(6080), 455–458.

Farley, K. A., E. G. Jobbágy, and R. B. Jackson (2005), Effects of afforestation on water yield: A global synthesis with implications for policy, *Global Change Biol.*, *11*(10), 1565–1576.

Felzer, B. S., T. W. Cronin, J. M. Melillo, D. W. Kicklighter, and C. A. Schlosser (2009), Importance of carbon-nitrogen interactions and ozone on ecosystem hydrology during the 21st century, *J. Geophys. Res.*, *114*(G1), 1–10, doi:10.1029/2008jg000826.

Felzer, B. S., T. W. Cronin, J. M. Melillo, D. W. Kicklighter, C. A. Schlosser, and S. R. Dangal (2011), Nitrogen effect on carbon – water coupling in forests, grasslands, and shrublands in the arid western United States, *J. Geophys. Res.: Biogeosci.*, *116*(G3), 1–23, doi:10.1029/2010JG001621.

Ferguson, C. R., J. Sheffield, E. F. Wood, and H. Gao (2010), Quantifying uncertainty in a remote sensing-based estimate of evapotranspiration over continental USA, *Int. J. Remote Sens.*, *31*(14), 3821–3865.

Field, C., R. Jackson, and H. Mooney (1995), Stomatal responses to increased CO_2: Implications from the plant to the global scale, *Plant Cell Environ.*, *18*(10), 1214–1225.

Fisher, J. B., K. P. Tu, and D. D. Baldocchi (2008), Global estimates of the land–atmosphere water flux based on monthly AVHRR and ISLSCP-II data, validated at 16 FLUXNET sites, *Remote Sens. Environ.*, *112*(3), 901–919, doi:10.1016/j.rse.2007.06.025.

Gedney, N., P. M. Cox, R. A. Betts, O. Boucher, C. Huntingford, and P. A. Stott (2006), Detection of a direct carbon dioxide effect in continental river runoff records, *Nature*, *439*(7078), 835–838, doi:10.1038/nature04504.

Glenn, E. P., A. R. Huete, P. L. Nagler, K. K. Hirschboeck, and P. Brown (2007), Integrating remote sensing and ground methods to estimate evapotranspiration, *Crit. Rev. Plant Sci.*, *26*(3), 139–168.

Hijmans, R. J., S. E. Cameron, J. L. Parra, P. G. Jones, and A. Jarvis (2005), Very high resolution interpolated climate surfaces for global land areas, *Int. J. Climatol.*, *25*(15), 1965–1978.

IPCC (2007), *Climate Change 2007: The Physical Science Basis Contribution of Working Group I to the fourth assessment report of the Intergovernmental Panel on Climate Change*, Cambridge Univ. Press, Cambridge, U. K.

Jackson, R. B., E. G. Jobbágy, and M. D. Nosetto (2009), Ecohydrology in a human – dominated landscape, *Ecohydrology*, *2*(3), 383–389.

Jung, M., et al. (2010), Recent decline in the global land evapotranspiration trend due to limited moisture supply, *Nature*, *467*(7318), 951–954, doi:10.1038/nature09396.

Kergoat, L., S. Lafont, H. Douville, B. Berthelot, G. Dedieu, S. Planton, and J. F. Royer (2002), Impact of doubled CO_2 on global – scale leaf area index and evapotranspiration: Conflicting stomatal conductance and LAI responses, *J. Geophys. Res.: Atmos. (1984-2012)*, *107*(D24), ACL 30-1–ACL 30-16, doi:10.1029/2001JD001245.

Klein Goldewijk, K., A. Beusen, G. Van Drecht, and M. De Vos (2011), The HYDE 3.1 spatially explicit database of human -induced global land - use change over the past 12,000 years, *Global Ecol. Biogeogr.*, *20*(1), 73–86.

Kurc, S. A., and E. E. Small (2004), Dynamics of evapotranspiration in semiarid grassland and shrubland ecosystems during the summer monsoon season, central New Mexico, *Water Resour. Res.*, *40*(9), 1–15.

Li, F., W. P. Kustas, J. H. Prueger, C. M. Neale, and T. J. Jackson (2005), Utility of remote sensing-based two-source energy balance model under low-and high-vegetation cover conditions, *J. Hydrometeorol.*, *6*(6), 878–891.

Liou, Y.-A., and S. K. Kar (2014), Evapotranspiration estimation with remote sensing and various surface energy balance algorithms—A review, *Energies*, *7*(5), 2821–2849.

Liu, M., H. Tian, G. Chen, W. Ren, C. Zhang, and J. Liu (2008), Effects of land - use and land - cover change on evapotranspiration and water yield in China During 1900–2001, *J. Am. Water Resour. Assoc.*, *44*(5), 1193–1207, doi:10.1111/j.1752-1688.2008.00243.x.

Liu, M., H. Tian, Q. Yang, J. Yang, X. Song, S. E. Lohrenz, and W. J. Cai (2013), Long-term trends in evapotranspiration and runoff over the drainage basins of the Gulf of Mexico during 1901-2008, *Water Resour. Res.*, *49*(4), 1988–2012, doi:10.1002/wrcr.20180.

Lockwood, J. (1995), The suppression of evapotranspiration by rising levels of atmospheric CO_2, *Weather*, *50*(9), 304–308.

Maurer, E., J. Adam, and A. Wood (2009), Climate model based consensus on the hydrologic impacts of climate change to the Rio Lempa basin of Central America, *Hydrol. Earth Syst. Sci.*, *13*(2), 183–194.

Meehl, G. A., C. Covey, K. E. Taylor, T. Delworth, R. J. Stouffer, M. Latif, B. McAvaney, and J. F. Mitchell (2007), The WCRP CMIP3 multimodel dataset: A new era in climate change research, *Bull. Am. Meteorol. Soc.*, *88*(9), 1383–1394.

Mohan, S., and N. Arumugam (1996), Relative importance of meteorological variables in evapotranspiration: Factor analysis approach, *Water Resour. Manage.*, *10*(1), 1–20.

Mu, Q., F. A. Heinsch, M. Zhao, and S. W. Running (2007), Development of a global evapotranspiration algorithm based on MODIS and global meteorology data, *Remote Sens. Environ.*, *111*(4), 519–536.

Mu, Q., M. Zhao, and S. W. Running (2011), Improvements to a MODIS global terrestrial evapotranspiration algorithm, *Remote Sens. Environ.*, *115*(8), 1781–1800.

Oki, T., and S. Kanae (2006), Global hydrological cycles and world water resources, *Science*, *313*(5790), 1068–1072, doi:10.1126/science.1128845.

Oleson, K., G. Y. Niu, Z. L. Yang, D. Lawrence, P. Thornton, P. Lawrence, R. Stöckli, R. Dickinson, G. Bonan, and S. Levis (2008), Improvements to the Community Land Model and their impact on the hydrological cycle, *J. Geophys. Res.: Biogeosci.*, *113*(G1), 1–20, doi:10.1029/2007JG000563.

Pan, S., H. Tian, S. R. Dangal, Z. Ouyang, B. Tao, W. Ren, C. Lu, and S. Running (2014a), Modeling and monitoring terrestrial primary production in a changing global environment: Toward a multiscale synthesis of observation and simulation, *Adv. Meteorol.*17 pp, doi:10.1155/2014/965936.

Pan, S., H. Tian, S. R. Dangal, C. Zhang, J. Yang, B. Tao, Z. Ouyang, X. Wang, C. Lu, and W. Ren (2014b), Complex spatiotemporal responses of global terrestrial primary production to climate change and increasing atmospheric CO2 in the 21st century, *PLoS One*, *9*(11), e112810, doi:10.1371/journal.pone.0112810.

Piao, S., P. Friedlingstein, P. Ciais, N. de Noblet-Ducoudré, D. Labat, and S. Zaehle (2007), Changes in climate and land use have a larger direct impact than rising CO2 on global river runoff trends, *Proc. Natl. Acad. Sci. U. S. A.*, *104*(39), 15242–15247.

Piao, S., et al. (2010), The impacts of climate change on water resources and agriculture in China, *Nature*, *467*(7311), 43–51, doi:10.1038/nature09364.

Porporato, A., F. Laio, L. Ridolfi, and I. Rodriguez-Iturbe (2001), Plants in water-controlled ecosystems: active role in hydrologic processes and response to water stress: III. Vegetation water stress, *Adv. Water Resour.*, *24*(7), 725–744.

Price, K. (2011), Effects of watershed topography, soils, land use, and climate on baseflow hydrology in humid regions: A review, *Prog. Phys. Geogr.*, *35*(4), 465–492.

Ren, W., H. Tian, B. Tao, Y. Huang, and S. Pan (2012), China's crop productivity and soil carbon storage as influenced by multifactor global change, *Global Change Biol.*, *18*(9), 2945–2957, doi:10.1111/j.1365-2486.2012.02741.x.

Rosolem, R., W. J. Shuttleworth, X. Zeng, S. R. Saleska, and T. E. Huxman (2010), Land surface modeling inside the Biosphere 2 tropical rain forest biome, *J. Geophys. Res.: Biogeosci. (2005–2012)*, *115*(G4), 1–19, doi:10.1029/2010JG001443.

Running, S. W., and J. C. Coughlan (1988), A general model of forest ecosystem processes for regional applications I. Hydrologic balance, canopy gas exchange and primary production processes, *Ecol. Modell.*, *42*(2), 125–154.

Seneviratne, S. I., D. Luthi, M. Litschi, and C. Schar (2006), Land-atmosphere coupling and climate change in Europe, *Nature*, *443*(7108), 205–209, doi:10.1038/nature05095.

Shams, S., S. Nazemosadat, A. K. Haghighi, and S. Z. Parsa (2012), Effect of carbon dioxide concentration and irrigation level on evapotranspiration and yield of red bean, *J. Sci. Technol. Greenhouse Cult.*, *2*(8), 1–10.

Shi, X., J. Mao, P. E. Thornton, F. M. Hoffman, and W. M. Post (2011), The impact of climate, CO_2, nitrogen deposition and land use change on simulated contemporary global river flow, *Geophys. Res. Lett.*, *38*(8), 1–6, doi:10.1029/2011GL046773.

Shi, X., J. Mao, P. E. Thornton, and M. Huang (2013), Spatiotemporal patterns of evapotranspiration in response to multiple environmental factors simulated by the Community Land Model, *Environ. Res. Lett.*, *8*(2), 024012, doi:10.1088/1748-9326/8/2/024012.

Tian, H., G. Chen, M. Liu, C. Zhang, G. Sun, C. Lu, X. Xu, W. Ren, S. Pan, and A. Chappelka (2010a), Model estimates of net primary productivity, evapotranspiration, and water use efficiency in the terrestrial ecosystems of the southern United States during 1895–2007, *For. Ecol. Manage.*, *259*(7), 1311–1327, doi:10.1016/j.foreco.2009.10.009.

Tian, H., M. Liu, C. Zhang, W. Ren, X. Xu, G. Chen, C. Lu, and B. Tao (2010b), The dynamic land ecosystem model (DLEM) for simulating terrestrial processes and interactions in the context of multifactor global change, *Acta Geogr. Sci.*, *65*, 1027–1047.

Tian, H., C. Lu, G. Chen, X. Xu, M. Liu, W. Ren, B. Tao, G. Sun, S. Pan, and J. Liu (2011a), Climate and land use controls over terrestrial water use efficiency in monsoon Asia, *Ecohydrology*, *4*(2), 322–340, doi:10.1002/eco.216.

Tian, H., J. Melillo, C. Lu, D. Kicklighter, M. Liu, W. Ren, X. Xu, G. Chen, C. Zhang, and S. Pan (2011b), China's terrestrial carbon balance: Contributions from multiple global change factors, *Global Biogeochem. Cycles*, *25*(1), 1–16, doi:10.1029/2010GB003838.

Trenberth, K. E. (2011), Changes in precipitation with climate change, *Clim. Res.*, *47*(1), 123–138, doi:10.3354/cr00953.

Trenberth, K. E., J. T. Fasullo, and J. Kiehl (2009), Earth's global energy budget, *Bull. Am. Meteorol. Soc.*, *90*(3), 311–323.

Vinukollu, R. K., R. Meynadier, J. Sheffield, and E. F. Wood (2011), Multi-model, multi-sensor estimates of global evapotranspiration: Climatology, uncertainties and trends, *Hydrol. Processes*, *25*(26), 3993–4010, doi:10.1002/hyp.8393.

Wei, Y., S. Liu, D. Huntzinger, A. Michalak, N. Viovy, W. Post, C. Schwalm, K. Schaefer, A. Jacobson, and C. Lu (2013), The North American Carbon Program Multi-scale Synthesis and Terrestrial Model Intercomparison Project–Part 2: Environmental driver data, *Geosci. Model Dev. Discuss.*, *7*(4), 2875–2893, doi:10.5194/gmd-7-2875-2014.

WHO/UNICEF (2003), *Global water supply and sanitation assessment: 2000 report* , pp. 1–87 , World Health Organization and UNICEF, Geneva, Switzerland.

Wigmosta, M. S., L. W. Vail, and D. P. Lettenmaier (1994), A distributed hydrology - vegetation model for complex terrain, *Water Resour. Res.*, *30*(6), 1665–1679.

Yan, H., S. Wang, D. Billesbach, W. Oechel, J. Zhang, T. Meyers, T. Martin, R. Matamala, D. Baldocchi, and G. Bohrer (2012), Global estimation of evapotranspiration using a leaf area index-based surface energy and water balance model, *Remote Sens. Environ.*, *124*, 581–595.

Yang, F., M. A. White, A. R. Michaelis, K. Ichii, H. Hashimoto, P. Votava, A.-X. Zhu, and R. R. Nemani (2006), Prediction of continental-scale evapotranspiration by combining MODIS and AmeriFlux data through support vector machine, *IEEE Trans. Geosci. Remote Sens.*, *44*(11), 3452–3461.

Yang, Q., H. Tian, X. Li, B. Tao, W. Ren, G. Chen, C. Lu, J. Yang, S. Pan, and K. Banger (2014), Spatiotemporal patterns of evapotranspiration along the North American east coast as influenced by multiple environmental changes, *Ecohydrology*, 1–12, doi:10.1002/eco.1538.

Yuan, W., S. Liu, G. Yu, J.-M. Bonnefond, J. Chen, K. Davis, A. R. Desai, A. H. Goldstein, D. Gianelle, and F. Rossi (2010), Global estimates of evapotranspiration and gross primary production based on MODIS and global meteorology data, *Remote Sens. Environ.*, *114*(7), 1416–1431.

Zeng, Z., S. Piao, X. Lin, G. Yin, S. Peng, P. Ciais, and R. B. Myneni (2012), Global evapotranspiration over the past three decades: Estimation based on the water balance equation combined with empirical models, *Environ. Res. Lett.*, *7*(1), 014026, doi:10.1088/1748-9326/7/1/014026.

Zhang, K., J. S. Kimball, R. R. Nemani, and S. W. Running (2010), A continuous satellite-derived global record of land surface evapotranspiration from 1983 to 2006, *Water Resour. Res.*, *46*(9), 1–21, doi:10.1029/2009wr008800.